




## Article

# A Closer Look at the Contact Conditions of a Block-on-Flat Wear Experiment

André Rudnytskyj<sup>1,2,\*</sup>, Roland Larsson<sup>3</sup> and Carsten Gachot<sup>2</sup><sup>1</sup> AC2T research GmbH, Viktor-Kaplan-Straße 2/C, 2700 Wiener Neustadt, Austria<sup>2</sup> TU Wien, Institute of Engineering Design and Product Development, Lehárgasse 6, BA Building 9th Floor, 1060 Wien, Austria; carsten.gachot@tuwien.ac.at<sup>3</sup> Division of Machine Elements, Luleå University of Technology, 97187 Luleå, Sweden; roland.larsson@ltu.se

\* Correspondence: a.rudnytskyj@gmail.com

† Current address: AC2T Research GmbH, Hafenstraße 47-51 Top A4.2, 4020 Linz, Austria.

**Abstract:** Specific wear rates of tribosystems always rely on the data obtained from wear experiments. Nonetheless, the events taking place during an experiment may often lead to wide variations and low repeatability of the results. In this work, the authors attempt to take a closer look into the dynamic contact conditions of a dry linearly reciprocating block-on-flat wear experiment. The finite element method and Archard's wear model are used through COMSOL Multiphysics<sup>®</sup> 5.2a and LiveLink<sup>™</sup> for MATLAB<sup>®</sup> software to model the wear and study the influence of different conditions of the block surface and alignment of the sample. Changes of the geometry of the block and the contact pressure are quantified for several back and forth motions, using an extrapolation scheme in the wear modelling methodology. The tracking of such changes allow a dynamic overview of how the block contact area and the contact pressure distribution change throughout time. The results show how the assumption of a constant contact area and use of a nominal contact pressure in calculating the wear rate in such experiments can be inappropriate, especially in the presence of roughness and misalignments of the block.

**Keywords:** wear modelling; block-on-flat; roughness; wear rate; Archard's equation; contact evolution; finite element method



**Citation:** Rudnytskyj, A.; Larsson, R.; Gachot, C. A Closer Look at the Contact Conditions of a Block-on-Flat Wear Experiment. *Lubricants* **2022**, *10*, 131. <https://doi.org/10.3390/lubricants10070131>

Received: 10 May 2022

Accepted: 17 June 2022

Published: 21 June 2022

**Publisher's Note:** MDPI stays neutral with regard to jurisdictional claims in published maps and institutional affiliations.



**Copyright:** © 2022 by the authors. Licensee MDPI, Basel, Switzerland. This article is an open access article distributed under the terms and conditions of the Creative Commons Attribution (CC BY) license (<https://creativecommons.org/licenses/by/4.0/>).

## 1. Introduction

Successful engineering applications often rely on the tribological performance of materials within their systems [1–3]. From hip prostheses [4] and DLC coatings [5] to NASA's Mars rover wheels [6], wear is often the focus of attention because of its drastic consequences if not predicted accurately. In terms of capital, a loss of as high as 6% of the annual U.S. gross domestic product was attributed to mechanical wear a few decades ago [7]. The common approach to characterize wear for predictions in applications is by means of standard tribological laboratory tests [8] and in terms of the specific wear rate  $k$ , calculated as

$$k = \frac{\Delta V}{Ld} \quad (1)$$

where  $\Delta V$  is the worn volume,  $L$  is the normal load, and  $d$  the sliding distance. Therefore,  $k$  is a dimensional wear coefficient with units  $\text{m}^3/\text{Nm}$ , which is assessed either in terms of mass loss or geometry change of the sample material being tested.

By characterising the wear of a material in a system using Equation (1), a series of complex physical and instrumental phenomena are being grouped together and implicitly represented by the parameter  $k$ . As a consequence, repeatability becomes challenging, which raises questions regarding the reliability of the results themselves. Recently, Watson and colleagues [9] have called attention to this matter by writing that, for ball-on-flat wear tests, about “21 tests would be required to estimate the mean worn volume, for a lab, with

5% standard error". Evidently, the non-equilibrium stochastic nature of a wear event [10] is partly to be blamed, but the experimental uncertainty of the instrumentation, such as misalignment of transducers, errors from voltage measurements, and aspects of the sample itself [11–14] are also playing a role, one which could be minimised by a more rigorous analysis and design of experiments.

In addition to a rigorous experimental set-up, modelling and simulation of the wear process can support the analysis of results. Computational tools can be used to shine light on variables that are not visible nor measured during the experiment, such as instantaneous contact pressure, slip velocity, and topography change. Such information can contribute to the understanding of the events taking place and possibly reduce the uncertainty in a measurement. This, of course, implies modelling the contact first, for which different approaches are available. The finite element method (FEM) is an attractive option—while it is true that FEM may be computationally much more expensive than other methods, such as the boundary element method [15], the FEM provides great versatility to include multiple physical phenomena [16]. In any case, the contact solution can subsequently serve as input to wear models [17]; the most used one, and practically a standard in the tribology community, is often referred to as *Archard's wear equation* (or Archard's law), which can be expressed by rewriting Equation (1) in a dynamic format as

$$\frac{dh(t)}{dt} = kp(t)v_s(t). \quad (2)$$

where  $t$  is time,  $p(t)$  is the contact pressure,  $v_s(t)$  is slip velocity, and  $h(t)$  is wear depth at the wearing surface (thus, the derivative is a height loss per unit time).

Although models have their own limitations, one of their advantages is not to have unknown physical factors affecting the results, since the equations representing the model are set by the programmer or user. Computational methods and models such as the FEM and Archard's wear model (or a modified version) have been broadly investigated in the literature [18–23], including for specific applications (e.g., gears [24]). Recently, Mukras [25] presented a thorough review of the literature on simulation and prediction of wear. Surprisingly few investigations have focused on the wear experiments themselves. Molinari et al. [26] studied a square cross-sectioned pin on disc involving heat transfer and thermo-plasticity; despite a complex physical scenario, the focus lied on the wear rate itself, and the physical time simulated was of 1 ms. Hegadekatte et al. [27] studied pin and disc wear in a pin-on-disc tribometer using Hertzian contact mechanics and small loads. A ball-on-disk experiment was analysed by Andersson et al [28], where the applicability of the Archard wear equation was questioned. A combination of FEM and the boundary element method was used by Ilincic et al. [29] to study a standardised reciprocating ball-on-disk experiment, where wear was modelled in both bodies; the authors show qualitatively good agreement but remark that a constant wear coefficient in a system might not be correct. A cylindrical flat punch was studied by Bortoleto et al. [30] from a macroscale point-of view; they compared experiments and simulations and found that the use of a wear coefficient obtained from experiments was not sufficient for the model to reproduce the experiment in terms of mass loss, possibly due to an overestimated wear coefficient, which included both steady-state and running-in regions.

It is well known that there are different stages of wear, and that a single coefficient will rarely describe them all. Furthermore, Equation (1) is too simple of an expression to account for other tribological aspects, such as lubrication or roughness, which may play a role in the wear rate [31]. Nonetheless, it is interesting to investigate the evolution of the contact conditions in an experiment to see if even under the assumption of a valid wear coefficient  $k$ , any other aspect is being overlooked. Such an investigation may be particularly critical if the wear coefficient is calculated based on a height change of the sample, which would imply that the contact area and therefore pressure are assumed to be constant.

In the current work, the authors take a closer look at the linearly reciprocating block-on-flat wear experiment (also named flat-ended pin-on-disc [32]) in an attempt to improve the understanding of wear and its measurement in such experiments. More specifically, the authors attempt to study how the presence of roughness on the block and misalignment of its holder affect the contact pressure and contact area, which would consequently have implications in the outcome of such experiments. The reciprocating wear test is interesting because of its dynamic conditions: the position, velocity, and acceleration of the block are functions of time, which leads to a dynamic contact pressure distribution, and consequently wear. To the best of the authors' knowledge, the block-on-flat wear experiment has not been explored in detail in the literature regarding the matters proposed in this work. Discrepancies between simulations and other experiments reviewed in the literature show there is room for investigation and that, even though regular wear experiments are just means to an end—namely the wear rate calculation—it might be useful to model the process to further put the assumptions of the calculation to the test.

## 2. Materials and Methods

The numerical model built in this work is based on a wear experiment in a linear reciprocating Cameron–Plint tribometer (Plint-TE77, Phoenix Tribology Ltd., Newbury, England). A scheme of the experiment is shown in Figure 1.

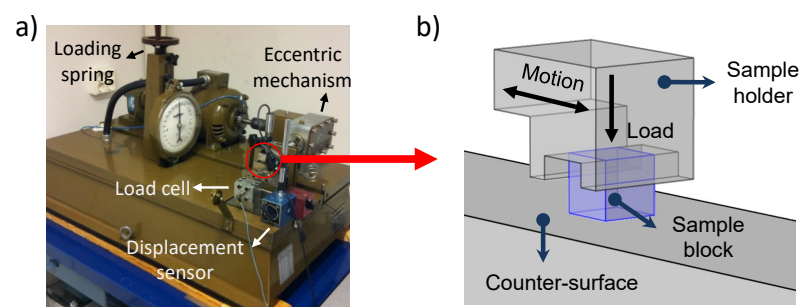


**Figure 1.** Cameron–Plint tribometer [33] on the (a), and scheme of experiment on the (b).

In such an experiment, a displacement sensor measures the vertical displacement of the sample block (i.e., the wear depth). The conditions are similar to those studied in [34]: the sample is a 4 mm cubic block that linearly reciprocates over a steel counter-surface with a stroke length of 5 mm and 0.5 Hz frequency under a constant normal load of 450 N. The nominal pressure is the load over the nominal area of 16 mm<sup>2</sup> (i.e., 28.125 MPa).

The experiment is modelled in a 2D space as shown in Figure 2. It consists of two domains: the sample block and the counter-surface. Although a faithful representation of the cubic block would require a 3D space, a 2D model is sufficient to explore the matters proposed in this work, and significantly reduces computational time. Plane strain conditions are used, and the thickness is set as 4 mm. Linear elasticity is used for the block, with Young's modulus, Poisson's ratio, and density of 3280 MPa, 0.39, and 1.4 g/cm<sup>3</sup>, respectively. These values are in the range of thermoplastic material commonly used as bearing material in hydropower applications [35]. Such materials are commonly self-lubricating, which leads to a dynamic tribosystem involving material transfer in the actual experiment, with a dynamic friction coefficient and wear rate; this aspect, however, lies outside the proposed scope of this work. The counter-surface material is a much harder steel, and therefore modelled as rigid. The lower edges of the block are filleted to resemble the sample of the experiment, which has important implications in the results, as discussed in Section 4. Referring to Figure 2, on (1), a boundary load (450 N) is applied on the block along with a spring foundation, which acts as a temporary weak spring to prevent rigid body motion of the block while contact is being established, since the domains are initially separated. The load is applied progressively in a stationary step using a parameter that also sets the spring to zero once the total load is reached, helping the solution to converge.

On (2), rigid connectors are applied on the upper parts of the block to represent the much stiffer holder and simulate the reciprocating motion using a sine wave for the displacement in the  $x$ -direction:

$$u(t) = B \sin(\omega t + \phi) \quad (3)$$

where  $B$  is the amplitude of the displacement—half the stroke— $\omega$  is the angular frequency of the motion, and  $\phi$  is the phase, which serves the purpose of defining the starting position of the block in the simulations, reducing computational time. A full back-and-forth motion lasts 2 s and is named a *cycle*. The load is applied in an initial stationary step, and the motion occurs in a time-dependent follow-up step.

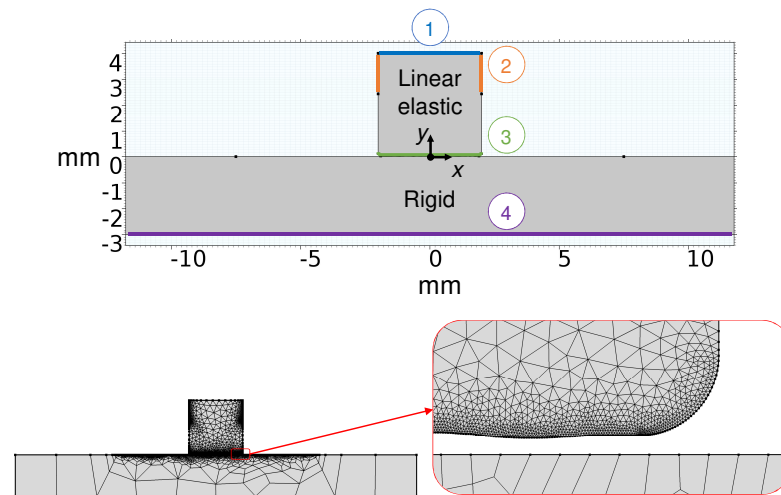


**Figure 2.** FEM model and indicated boundary conditions, and FEM mesh detailed below.

Archard's wear Equation (2) is defined on the block's contacting boundary (3) as a boundary ordinary differential equation to be solved in the simulations, using the contact pressure and slip velocity from the solution of the contact problem. The contact pair is a *source/destination* pair, meaning the *destination* (or *slave*) boundary (i.e., the block boundary) is constrained not to penetrate the *source* (or *master*) boundary (i.e., the counter-surface). Penalty formulation is used in the contact, which essentially means that a stiff spring active only in compression is inserted between the contacting boundaries. The penalty factor is set as default by the software, namely the stiffness of the material over the minimum mesh size of the destination boundary.

The counter-surface is fixed on its bottom (4) and treated as a rigid body. Since the counter-surface is assumed rigid and the block's lower boundary is constantly in contact, wear is modelled only on the block. A constant dimensional wear coefficient ( $4.78 \times 10^{-15} \text{ Pa}^{-1}$ ) and friction (Coulomb model with constant coefficient of 0.06) are inputs to the model, taken from a previous work [36]. The wear depth is calculated and used to update the geometry. In including friction, the tangential force vector is added as a force variable, which was computed using the penalty formulation with the same settings for the contact. The sticking condition is thus replaced by a stiff spring. No regularization [37] is performed with regards to slip in the friction algorithm; the slip is approximated using a backward Euler step based on the mapped coordinates in the last converged time step. It was verified that there were no instabilities from the friction model, which can be attributed to the sufficiently refined finite element mesh and robustness of the algorithm implemented in the software. Inertial effects were verified to be negligible, so they were not considered in the simulations.

A typical finite element mesh is shown in Figure 2. The mesh on the block boundary is greatly refined in order to accurately represent the geometry and capture changes in this geometry due to wear. The FEM is used by means of the commercial software

COMSOL Multiphysics® 5.2a, and the geometry update is controlled using the LiveLink™ for MATLAB®.

### 2.1. Geometry Update

Once contact variables and wear are quantified, the next step in the methodology is the change of the geometry due to wear. The geometry update of the block is performed by assuming the block wears perpendicularly to the counter-surface, similarly to other works [21], which is assumed to be reasonable given the configuration of the system. Thus, the geometry update is in fact an update of the vertical coordinates of points composing the block's contacting boundary. The amount of these points depends on the size of the finite element mesh, which is rebuilt after every geometry update, but with a generally similar size throughout the simulations. In this sense, the methodology is somewhat different to that performed in [36], since the points can vary with the size of the mesh. The block is rebuilt with the updated coordinates by linearly interpolating the points into a continuous boundary.

The geometry update can be mathematically expressed with a temporal discretization of Equation (2) as the following:

$$h_{j,i+1} = h_{j,i} + \Delta h_{j,i}, \quad \text{where } \Delta h_{j,i} = \Delta t_g k p_{j,i} v_{s,j,i} \quad (4)$$

where  $j$  is the current cycle,  $i$  is the current time step in this cycle, and  $h_{j,i}$  is the current vertical coordinate (corresponding to the  $y$  direction) of a point in the geometry. The term  $\Delta h_{j,i+1}$  is the wear increment, which equals the time interval after which the geometry is updated ( $\Delta t_g$ ), the wear coefficient  $k$ , the contact pressure  $p_{j,i+1}$ , and the slip velocity  $v_{s,j,i+1}$ . Given the  $y$  coordinate orientation, the wear increment corresponds to a positive update of the  $y$  coordinate value; hence, the wear increment is added to  $h_{j,i}$ . In this sense, the simulation of the experiment is a series of simulations of time duration  $\Delta t_g$ , after which the geometry is updated.

In order to visualise the evolution of the geometry and contact conditions in a reasonable number of simulations, a common approach is to use an extrapolation factor  $A$  that multiplies the wear increment. In practice, this means that the wear coefficient is artificially increased by a factor  $A$ , or that  $A$  number of cycles are represented per simulated cycle. In any case, the extrapolation factor presumably allows one to visualise the evolution of the geometry while reducing the number of simulations. One of the challenges in this methodology is how to maintain a reliable update of the geometry with  $A$  and  $\Delta t_g$ . Different approaches are found in the literature. The criterion used by Mukras [38] was that there should be "smooth pressure distribution" at every update. Cha et al [39] used a procedure to smooth the worn surface and therefore avoid unrealistic worn shapes. Põdra and Anderson [40] set a "maximum allowed wear increment (...) predefined on the basis of experience and adjusted to as large as possible by making short simulation test runs.". Due to the lack of a well-defined criterion, this work also performed tests and adjusted  $A$  and  $\Delta t_g$  in order to obtain a subjectively smooth and stable geometry evolution. Values of  $A = 500$  and  $\Delta t_g = 0.1$  provided reasonable results and are used throughout the simulations.

### 2.2. Situations

As shown in Figure 3, three surface profiles for the block's contacting boundary were analysed: a flat surface, a surface with a small bump, and a rough surface.

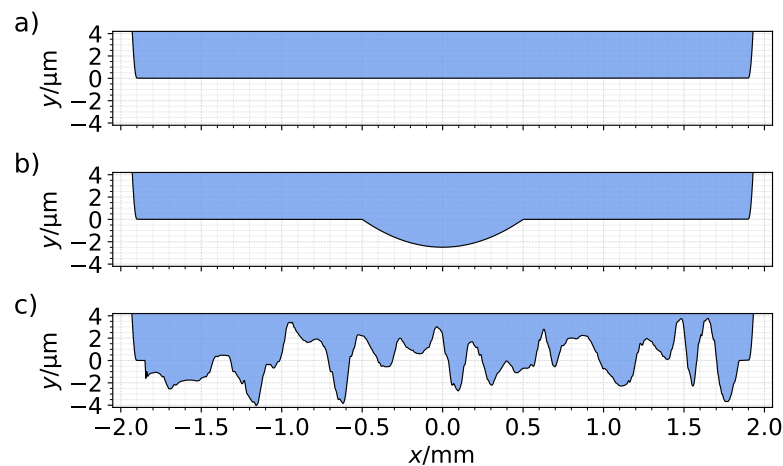


**Figure 3.** Block bottom boundaries (which contact counter-surface) studied in this work: (a) flat, (b) bumped, (c) rough. Solid region is shown in blue.

The flat surface represents the ideal nominally flat situation where the contact area of the block would equal the nominal contact area. The bumped surface contains a parabolic protuberance of 1 mm wide and a couple of micrometers in height located in the middle of the otherwise flat profile. The rough surface is a cross section from an artificially generated random isotropic 3D topography, similar to the one used in [16]; it is inserted between  $x = -1.85$  mm and  $x = 1.85$  mm and has an average roughness of  $1.53$   $\mu\text{m}$  in this interval. The three surfaces are identical at the edges (i.e., for  $|x| > 1.85$  mm).

Three holder situations are studied: aligned, tilted, and loose. The aligned situation means that the rigid connectors (Figure 2) representing the holder are perpendicular to the counter-surface at all times. The tilted condition corresponds to a misaligned situation in which a clockwise tilt of  $0.5^\circ$  is imposed by the holder, which intends to mimic a misaligned sample holder or a sample fixed not perfectly straight. The loose situation corresponds to a  $0.5^\circ$  clockwise tilt when moving to the right, and  $0.5^\circ$  counter-clockwise when moving to the left, as if the sample holder would be slightly loose such that it allows a small rotation depending on the movement direction. Alternatively, it can be thought of as the compliance of the system. These conditions are applied in the FEM model by imposing a prescribed rotation on the rigid connectors of the block.

### 3. Results

Simulations for the three surfaces under each holder condition were performed using an extrapolation factor of  $A = 500$  and a geometry update time interval of  $\Delta t_g = 0.1$  for a total of 8 cycles. The simulation starts with the block moving to the right. If  $A$  is interpreted to represent several cycles per simulated cycle, this would correspond to a total of 4000 cycles, or 2.22 h of experiment. The nominal pressure of the experiment is used as a reference to normalize the results (i.e.,  $p_n = p_r = 28.125$  MPa).

#### 3.1. Flat Block

In a static and frictionless contact, the flat block resembles a flat-ended indenter as discussed by [41], in which the contact pressure sharply increases towards the edges and is in fact undefined at the very edge if the corner is perfectly sharp [42]. Filletting the edge allows a smoother increase, but the sharp peak remains because the fillets are rather small and a true continuity between flat and rounded regions is not possible due to the discretized geometry. In case of the reciprocating block, the holder forcing the motion from the upper part of the block combined with the friction forces at the bottom of the block act in such a way as to “twist” it towards the leading edge of the movement, increasing the contact pressure at that side. Thus, the pressure distribution becomes somewhat asymmetric, with

the higher pressure peak in the leading edge. Figure 4 shows the flat surface profile and corresponding contact pressure at the start of the simulations.

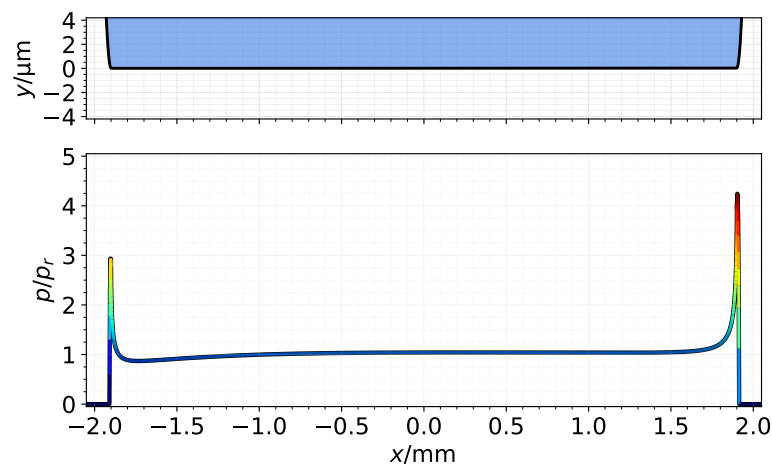


**Figure 4.** Normalized contact pressure for aligned flat block at initial geometry (i.e., start of simulations; block moving to the right).

The evolution of pressure and geometry due to wear is shown in Figure 5; the “Cycle” axis can be thought of as a time axis, with each cycle corresponding to a full back and forth motion with the extrapolated wear increment.

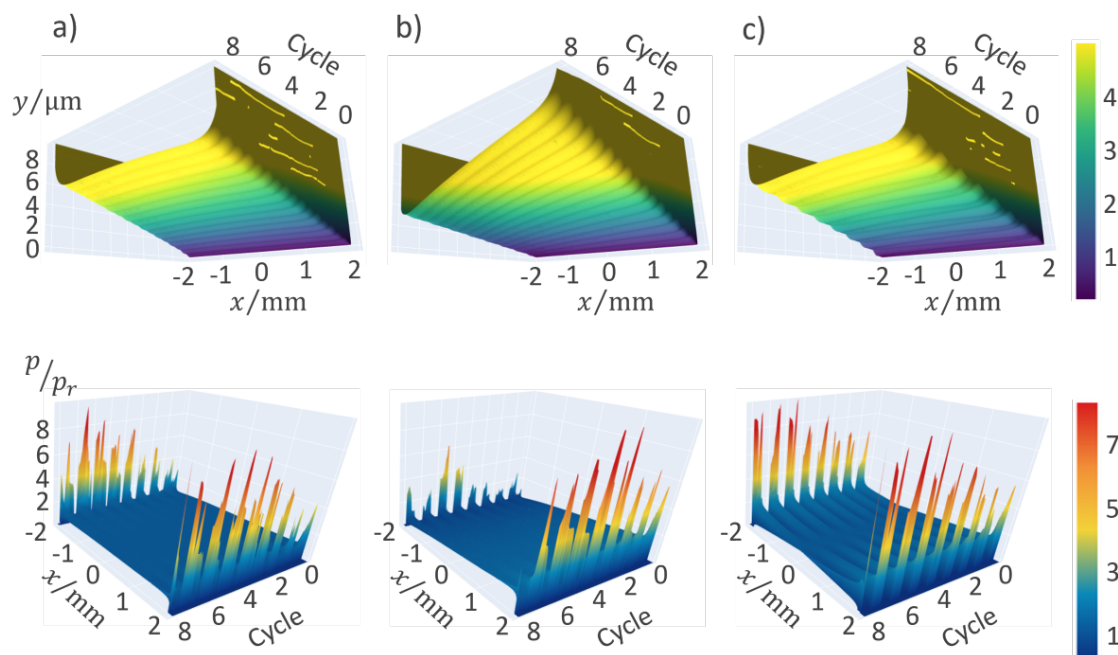


**Figure 5.** Geometry of flat block throughout 8 cycles corresponding to 2.22 h of experiment: (a) aligned, (b) tilted, (c) loose. Corresponding contact pressure shown below.

Figure 5 shows that the pressure peaks in the leading edges remain and may also increase throughout the cycles. Within a cycle, the peaks were observed to decrease as the block moves, but every change in the motion direction was accompanied by a sudden pressure peak at the leading edge. Overall, the pressure is relatively constant in most of the contact, which causes the block to remain generally flat. A “wavy” pattern is visible in the geometry, particularly in the loose case; this is a result of the reciprocating motion of

the block, which causes it to wear more in the middle of the cycle, when the velocity is the highest. The final geometry of each case is compared in Figure 6.

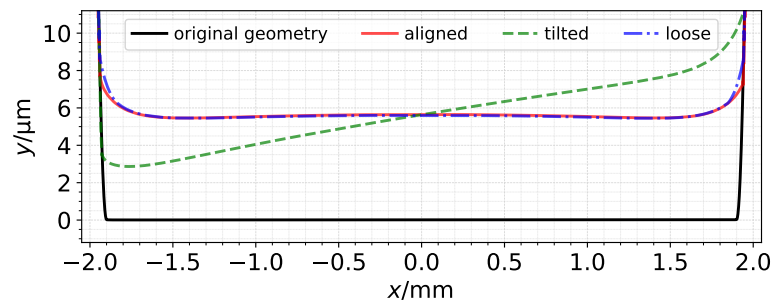


**Figure 6.** Final geometry of flat block under different conditions at the end of simulations.

Not surprisingly, the tilted condition resulted in more wear at the side tilted towards the counter-surface (positive  $x$  values) and less at the opposite side. More surprisingly, the loose condition resulted in a very similar final geometry to that of the perfectly aligned case. This can be attributed to the compensation that occurs due to the reciprocating motion: while moving in one direction, the block is tilted towards the counter-surface at one side, and consequently wears more at that side; while returning (i.e., in the second half of the cycle), the block is tilted the other way, wearing more intensely the opposite side. A rounding of the edges is also seen in all cases, which can be attributed to the pressure peaks.

### 3.2. Bumped Block

Even though a bump in the block initially contacts the counter-surface first, the deformation of the material under the relatively high load causes the whole surface of the block to get in contact, as shown in Figure 7. Consequently, the characteristic contact pressure peaks at the edges are present also in this case. It is reasonable to assume that a larger bump could eventually reduce or even avoid contact of the edges, which would render completely different results.

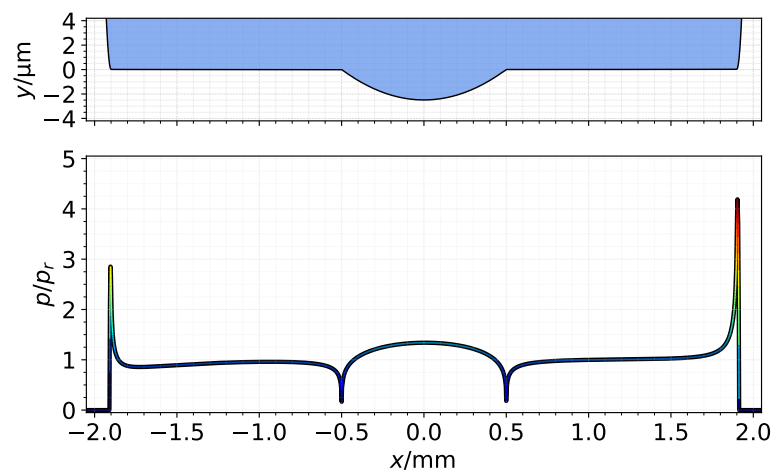


**Figure 7.** Normalized contact pressure for aligned bumped block at initial geometry (i.e., start of simulations; block moving to the right).

Figure 8 shows that, even though the bump is visible throughout the simulations, it decreases in size and causes the pressure peaks at the edges to intensify. After some time, the block essentially behaves as a flat block. Figure 9 shows the surface of the block after 8 cycles and how the bump has practically worn away. For the same reasons as in the flat block case, the aligned and loose bumped blocks' geometry are virtually indistinguishable



after 8 cycles, whereas the tilted block wears out preferentially at the side tilted towards the counter-surface.

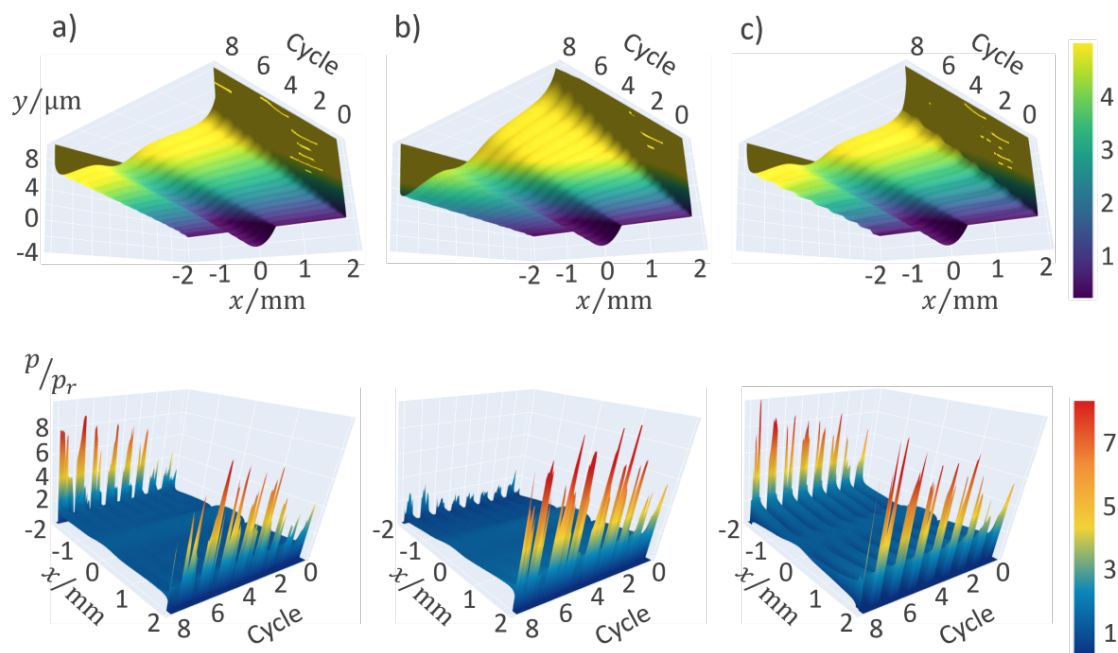


**Figure 8.** Geometry of bumped block throughout 8 cycles corresponding to 2.22 h of experiment: (a) aligned, (b) tilted, (c) loose. Corresponding contact pressure shown below.

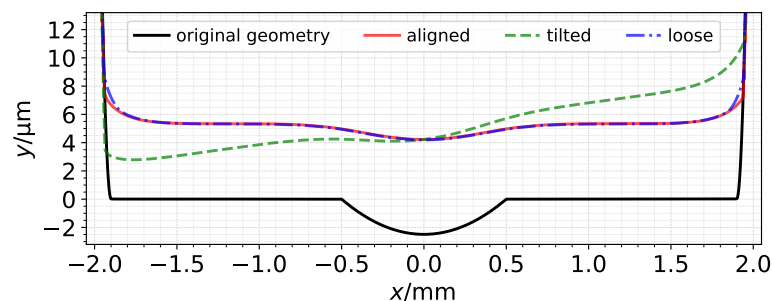


**Figure 9.** Final geometry of bumped block under different conditions at the end of simulations.

### 3.3. Rough Block

The rough block is particularly interesting because of its variety of contact pressures, and dynamic geometry change. Figure 10 shows the initial rough surface and corresponding contact pressure.

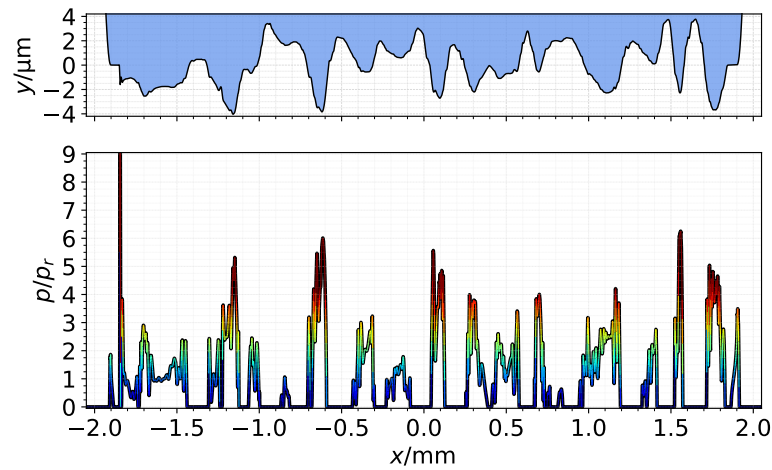


**Figure 10.** Normalized contact pressure for aligned rough block at initial geometry (i.e., start of simulations; block moving to the right).

As one would expect, the highest asperities support the highest contact pressures, while some of the valleys do not even contact the counter-surface at the start. Evidently, the total area of the block contacting the counter-surface is dependent on the material properties and the external load. Since the geometry is rough, the pressure peaks at the edges due to the twist effect are not as obvious as in the previous cases, but an analysis of the static contact in comparison to when the block starts to move showed that it was indeed present, slightly increasing the pressure at the peaks of the leading edge of the block, and decreasing at the rear. The highest pressure peak at around  $x \approx -1.85$  is due to a very sharp geometry change at this position, which corresponds to the end of the rough profile; as shown in the evolution of the geometry and contact pressure in Figure 11, this and other pressure peaks vanish as the geometry smooths out.

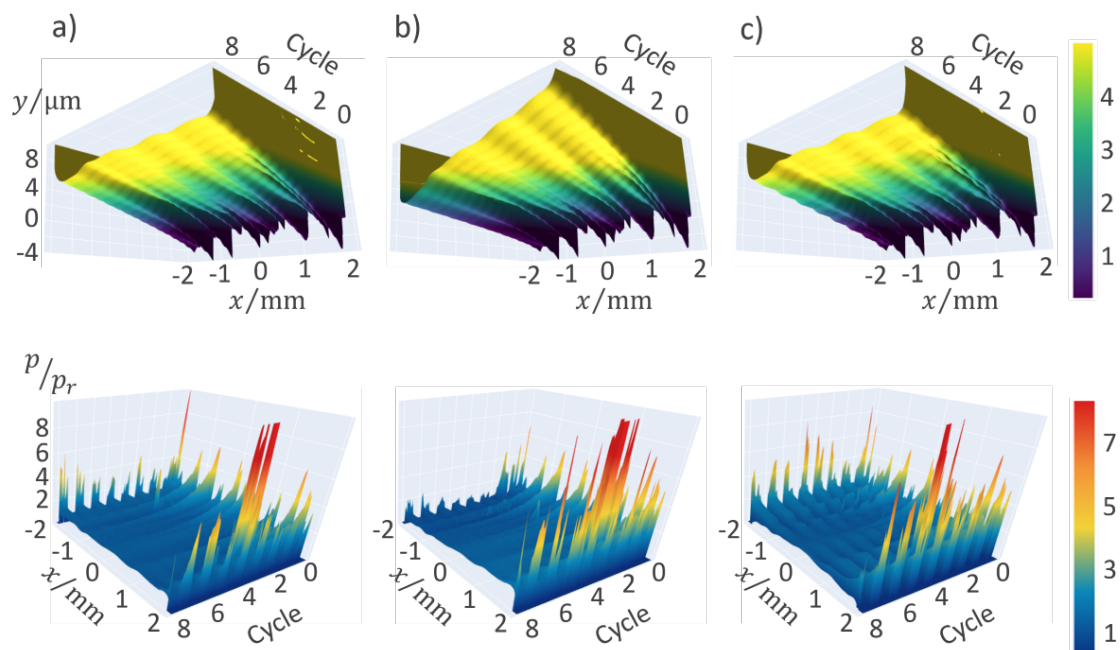


**Figure 11.** Geometry of block throughout 8 cycles corresponding to 2.22 h of experiment with initial rough surface: (a) aligned, (b) tilted, (c) loose. Corresponding contact pressure shown below.

The highest peaks result in the highest contact pressures and are therefore the surface features that wear first. After about 2 cycles, a high pressure peak unexpectedly showed up; this was verified to be due to a very sharp geometry lasting a few steps after a geometry update. Such events are likely unrealistic and a consequence of the wear model methodology, in which the geometry update at one point may create an unreasonable sharp geometry at the neighbouring points, leading to very high pressures. A few options are possible to deal with such problems, which have been used by other authors: reducing the time step for the geometry update, reducing the extrapolation factor (or using an adaptive factor), limiting the maximum wear increment, smoothing the geometry after the update, and so on. Here, since there was no unstable development in subsequent updates, meaning the routine was robust enough to deal with these “disturbances”, no corrective measures were necessary. The contact pressure becomes smoother and more uniform until the geometry is flat enough to create the typical pressure peaks at the edges of the block.

Figure 12 shows the geometry of the rough block after 8 cycles. Once again, the aligned and loose cases showed no significant difference, while the tilted situation caused the block geometry to wear preferentially at the side tilted towards the counter-surface. Despite the rough start, the geometry smooths out to such a degree that only a glimpse of the roughness remains, but it no longer causes significant changes in the pressure distribution.

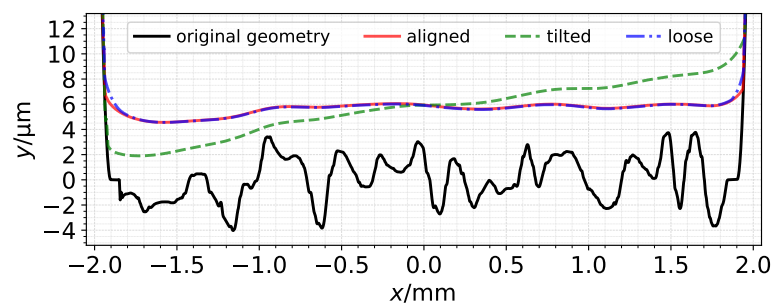


**Figure 12.** Final geometry of rough block under different conditions at the end of simulations.

## 4. Discussion

### 4.1. Contact Area

In the experiment, on which the FEM model is based in this work, the vertical displacement of the sample block is measured throughout the test. This vertical displacement is considered to be the wear depth, and the specific wear rate is calculated as the slope of the wear depth against  $p_n d$  (i.e., against nominal pressure  $p_n$  times distance  $d$ ). In other words, the pressure and contact area are assumed to be constant and equal to the nominal values, that is,  $p_n = 28.125$  MPa and  $A_n = 16$  mm<sup>2</sup>, respectively.

Figure 13 shows the normalized contact area for the flat block throughout the 8 cycles. In reality, the *contact length* was computed, and a nominal contact length of 4 mm was used, since it is a 2D model. In any case, one can see that the contact length or area does not remain constant.

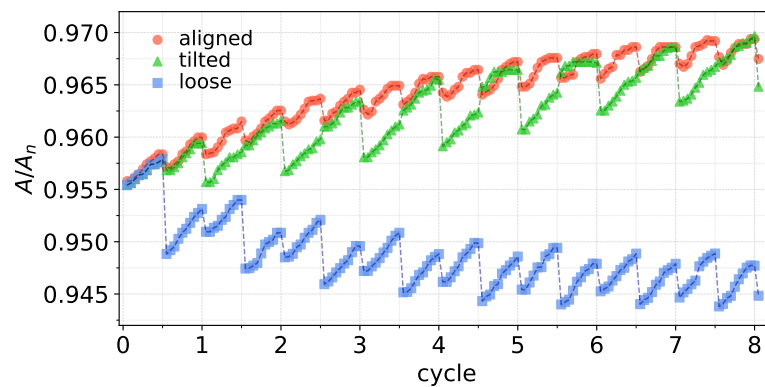


**Figure 13.** Contact area of flat block under different conditions after 8 cycles corresponding to 2.22 h of experiment.

It should be noted that due to the filleting of the edges of the initial block geometry, the initial contact area is about 0.045% smaller than the nominal one and could have been taken as the reference value just as well. While the block is moving in the same direction, the wear causes the contact area to increase, whereas a change in the direction of movement causes a sudden drop. Evidently, this occurs because the block is less worn on the rear side of the movement, and the change in direction twists the block towards this side, resulting in less contact area overall. While an increase in the contact area due to wear may seem obvious when the surface is rough, the increase in the flat block should be clarified.

Figure 14 shows the edge region in detail and reveals how the contact area increases towards the edge due to wear of the initially filleted region. On the right image, one can see that the pressure distribution is initially limited to  $x \approx 1.92$ , but reaches  $x \approx 1.94$  at the end of the simulations. Thus, the increase in the contact area is only possible as long as there is a curved region that can be worn out to increase the contact area, and therefore the contact area is expected to stabilize once this region is worn away; if the fillet was non-existent, the contact area would presumably not change. The geometry of the edge region also shows that the initially filleted geometry transforms into a kind of saw-tooth profile before being flattened; this is a consequence of the high pressure peaks leading to large changes in the geometry update, causing neighbouring points to stably alternate in the supporting of the high pressures. As a result, a microscale saw-tooth-like profile develops, which appears round when seen from a distance, as in Figure 6.

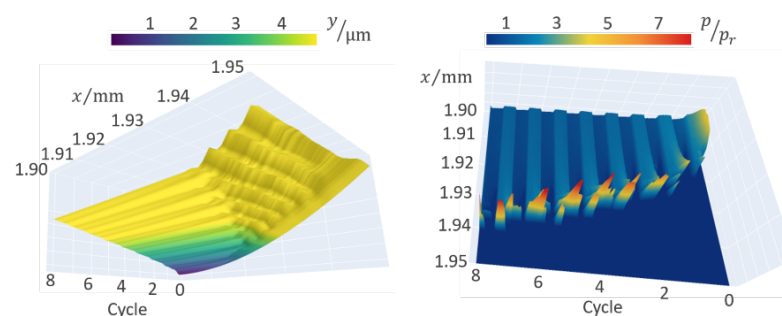


**Figure 14.** Edge region of aligned flat block (left) and corresponding pressure distribution (right) throughout 8 cycles.

Even though the final surface of the flat block under loose conditions was previously observed to be practically the same as the aligned case after 8 cycles (Figure 6), a difference of around 0.02% can exist in the contact area between the two cases. Such difference is due to the way the edge region changes in each case. Even though such small differences can generally be considered negligible, it is important to highlight that the results of 8 extrap-

olated cycles presented here would correspond to an experiment lasting approximately 2.22 h and a very small misalignment of  $0.5^\circ$ , whereas wear tests can last several more hours or even days, and larger or unstable misalignment can occur. Therefore, depending on the geometry and holder conditions, differences observed in each case may intensify with time and therefore become increasingly significant.

A more critical case is that of the rough block, shown in Figure 15.

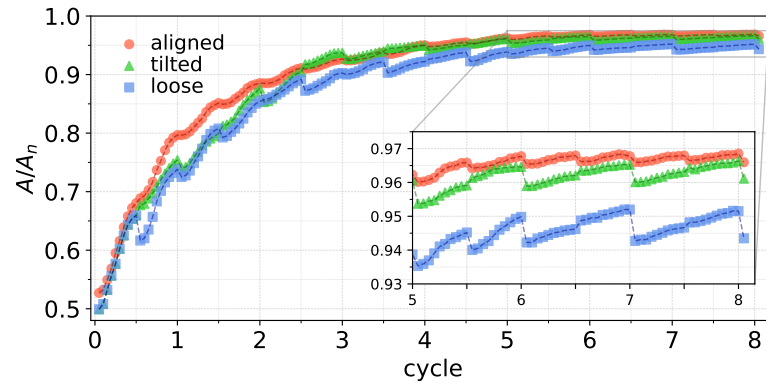


**Figure 15.** Contact area of rough block under different conditions after 8 cycles corresponding to 2.22 h of experiment. Results between cycles 5 and 8 are detailed in zoomed-in box.

The roughness of the block results in an initial contact area of approximately half of the nominal, which increases through time until it stabilizes and resembles the flat block. Although the overall behaviour is not surprising, the simulations allow to see and quantify the increase of the contact area with time. This tracking allows one to assess the amount of time needed to reach certain thresholds, which can be associated with particular events in the experiments. The time and length for the block to reach the steady-state contact area according to some criterion in Figure 15 could be associated with the running-in period in an actual experiment, which can now be predicted with the aid of the model. Alternatively, the model can inform how long a test should be run until steady-state conditions are expected to be reached.

#### 4.2. Contact Pressure

Since the load is constant, changes in the contact area result in changes in the contact pressure. As shown in Section 3, the pressure can be quite varied even for the aligned flat block. To better visualise how distributed the pressure is, Figure 16 shows a bi-dimensional histogram for the aligned flat block, where a pressure frequency distribution is performed for each time step. Thus, the log scale colormap represents the number of counts in each pressure bin, sized at 0.01 MPa. Additionally, an estimated distribution density using a Gaussian kernel [43] is plotted for the start of the simulations and for the end, which helps to see how the pressure distribution has changed over the analysed time; to avoid that, the curve extends to negative values, and the density is truncated at zero, meaning it is evaluated only for positive values.

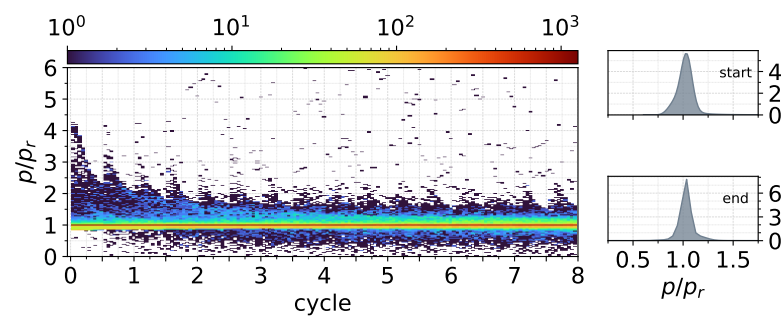


**Figure 16.** Normalized pressure frequency distribution for aligned flat block throughout simulations and kernel density estimate of the start and end.

The figure above shows how the pressure distribution changes, particularly during the first two cycles, where the distribution is skewed to values greater than 1. The high pressure peaks at the edges of the block presented previously are evidenced again in Figure 16 by the few bins at high pressure values. However, it is possible to see now that these high pressure values comprise only a very small portion of the pressure counts, whereas the great majority indeed concentrate around the nominal value. The density plot also shows that the distribution does not change much from start to end, except for a further concentration around the expected nominal value. Nonetheless, we see that even under ideal conditions of a perfectly aligned and flat surface, the pressure distribution comprises a range of values around the assumed nominal value.

Evidently, the results change when the block is slightly tilted or loose. Figure 17 shows the distribution for the tilted and loose flat block. The tilted block clearly shows the effects of the change in motion direction, with a visible change in the distribution occurring in the middle and end of every cycle. Interestingly, the distribution is more contained when the block moves to the left. In general, however, the pressure values are not as concentrated as in the aligned case, evidenced by the significant number of counts lying around the nominal value. The spread is also large in the loose case, but without any noticeable difference due to motion direction. Figures 18 and 19 show the same analysis for the bumped and rough block, respectively.

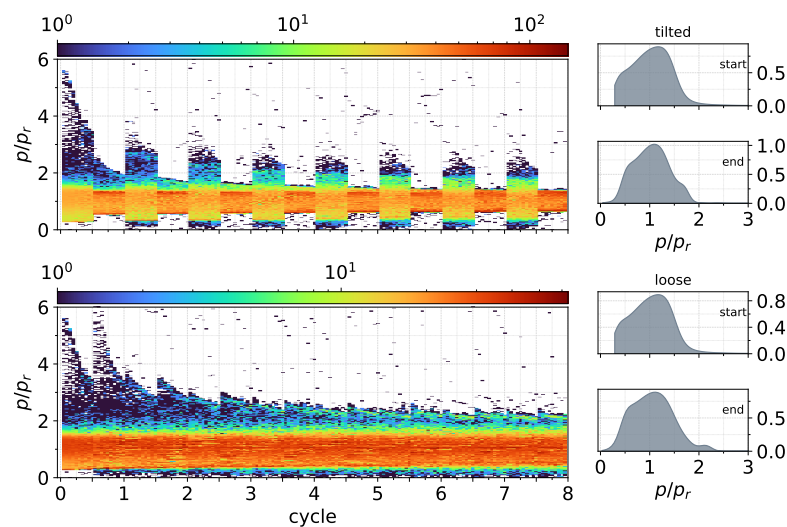


**Figure 17.** Normalized pressure frequency distribution for tilted (**top**) and loose (**bottom**) flat block throughout simulations and kernel density estimate of the start and end.

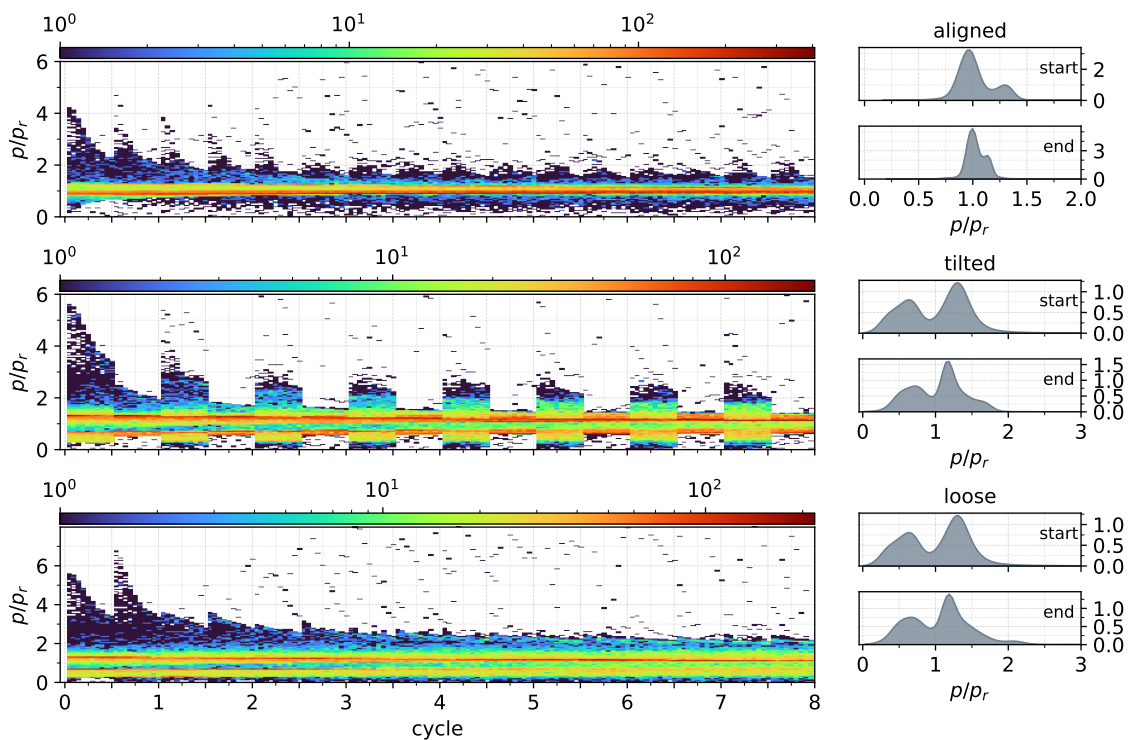


**Figure 18.** Normalized pressure frequency distribution for bumped block throughout simulations: aligned (**top**), tilted (**middle**), and loose (**bottom**).

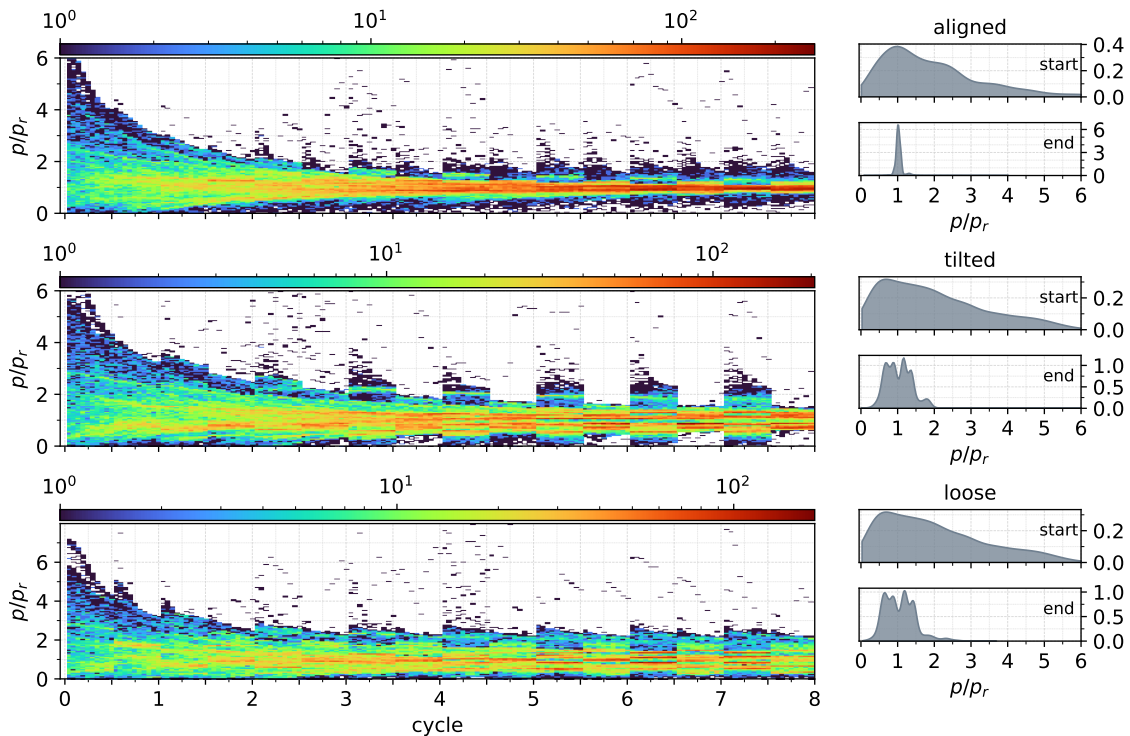


**Figure 19.** Normalized pressure frequency distribution for rough block throughout simulations: aligned (**top**), tilted (**middle**), and loose (**bottom**).

The bumped block analysis reveals that the bump has an important effect: it causes the pressure to concentrate in two different bins. When the block is tilted or loose, this effect is intensified in such a way that the peaks are located around the nominal value and not on

it. The distribution of the rough block simulations shows once again its highly dynamic process, with a very wide distribution during the initial cycles, eventually reaching an apparent steady state after a few cycles. It is seen once again that tilted or loose conditions lead to much wider distributions, whereas aligned conditions present similar final results for the studied surfaces.

#### 4.3. Implications for Experiments

The specific wear rate in the block-on-flat wear experiment is calculated as the slope of height loss over the nominal pressure times sliding distance. We see now that this pressure is entirely dynamic, to a greater or lesser extent depending on the holder situation, surface roughness, and time period. Clearly, the discretization of the geometry, time, sensitivity in the geometry update, and extrapolation factor add a lot of simplifications to the numerical model. Nonetheless, the results based on this numerical model provide insights on aspects that could be looked at in further detail. In this sense, the investigations showed that an alignment and stiff holder is critical for reducing the spread of the pressure distribution; when the block is aligned, all three surfaces eventually reached a very similar and concentrated pressure distribution, meaning they all eventually behave as a flat block. This, however, takes some time, and this aspect should be taken into consideration when analysing the results and calculating wear rate.

If the block is slightly tilted or loose, this showed relevant effects on the pressure distribution, even if the contact area varies very little. An entirely stiff holder or machine is unrealistic, since there will always be some compliance of the parts. Thus, misalignment resulting in tilting or additional movements of the sample are likely to occur. The standard deviation of the normalized pressure distribution at the end of the simulations for the flat block in tilted and loose conditions were quantified to be 0.36 and 0.45, respectively, which shows that a wide range of pressures is present.

The results have also shown that when irregularities are present in the sample block, which will always be the case, additional effects may occur. Although the intensity of this effect likely depends on the length scale of such irregularities, the roughness in the micrometer range studied in this work is realistic. The bumped block results seen in Figure 18 are clearly different from the aligned cases, showing two peaks of pressure counts and non-Gaussian distributions. The rough block also ended up in a rather particular distribution, starting out from a wide distribution. As discussed previously, roughness also has the additional aspect of highly dynamic contact conditions prior to reaching steady-state conditions.

In this sense, instead of referring to the constant nominal pressure of a wear experiment, perhaps it would be more accurate to talk about a *pressure distribution* of a wear experiment. By using statistical parameters, the distribution could be characterised, and differences seen in similar experiments could be better explained. If the experiment is to represent a specific application, and roughness is not explicitly included in the calculation of a wear rate, then using samples with the same surface topography as that in the actual application for which the experiment was set could minimise the uncertainty. Nonetheless, this would also require that the actual loading conditions are used, which implies knowing and considering the effects of the compliance of the system.

In addition to the wear analysis, friction is often measured simultaneously in such wear tests. The implications regarding the non-uniform pressure distribution, running-in period, and compliance of the system evidently apply to the friction measurement as well, especially when considering that friction is rarely measured directly at the interface.

## 5. Conclusions

In this work, modelling of a linearly reciprocating block-on-flat wear experiment was used to quantify the changes in the contact conditions during such a test. The simulations of different conditions of the block's wearing geometry in terms of surface profile and



alignment resulted in an analysis of the contact area and contact pressure distribution through time, allowing the following conclusions to be made:

- The FEM and wear model representing the block-on-flat wear experiment in this work reveal that, despite its assumptions and relative simplicity, rather complex contact conditions can occur in such an experiment.
- Roughness has important effects on the contact area and pressure distribution, both of which change dynamically for a significant period of time before reaching steady-state conditions. In apparent steady conditions, and therefore a less rough profile, the remaining unevenness of the roughness might still result in a wide pressure distribution if tilting or compliance are present.
- Alignment and stiffness of the sample holder is paramount for achieving a concentrated pressure distribution around the nominal value, which is assumed in the calculation of the specific wear rate by means of wear depth measurement. Regardless of the surface profile, slight misalignment or compliance of the system will widen and change the distribution significantly, which may persist throughout the entire experiment.
- The specific wear rate for tribological systems could be more accurately estimated and better understood by using numerical models alongside experiments, which allows one to visualise the contact conditions throughout the duration of the test.

**Author Contributions:** Conceptualization, A.R. and R.L.; methodology, A.R.; software, A.R.; formal analysis, A.R.; investigation, A.R.; visualization, A.R.; supervision, R.L. and C.G.; writing—original draft preparation, A.R.; writing—review and editing, A.R., R.L. and C.G. All authors have read and agreed to the published version of the manuscript.

**Funding:** Part of this work was supported by the Austrian COMET-Program (K2 Project InTribology, no. 872176) and carried out at the “Excellence Centre of Tribology” (AC2T research GmbH). Open Access Funding by TU Wien. The authors acknowledge TU Wien Bibliothek for financial support through its Open Access Funding Programme.

**Data Availability Statement:** The data presented in this study are available upon request from the corresponding author.

**Acknowledgments:** The authors thank the EACEA agency and its support in the Joint Master Programme in Tribology of Surfaces and Interfaces—TRIBOS. Some of the data and images in this work were processed and created by means of free and open-source software [44,45].

**Conflicts of Interest:** The authors declare no conflict of interest. The funders had no role in the design of the study; in the collection, analyses, or interpretation of data; in the writing of the manuscript, or in the decision to publish the results.

## References

1. Popov, V.L. Is Tribology Approaching Its Golden Age? Grand Challenges in Engineering Education and Tribological Research. *Front. Mech. Eng.* **2018**, *4*, 16. [CrossRef]
2. Meng, Y.; Xu, J.; Jin, Z.; Prakash, B.; Hu, Y. A review of recent advances in tribology. *Friction* **2020**, *8*, 221–300. [CrossRef]
3. Vellwock, A.E.; Yao, H. Biomimetic and bioinspired surface topographies as a green strategy for combating biofouling: A review. *Bioinspiration Biomim.* **2021**, *16*, 041003. [CrossRef] [PubMed]
4. Innocenti, B.; Labey, L.; Kamali, A.; Pascale, W.; Pianigiani, S. Development and Validation of a Wear Model to Predict Polyethylene Wear in a Total Knee Arthroplasty: A Finite Element Analysis. *Lubricants* **2014**, *2*, 193–205. [CrossRef]
5. Zellhofer, M.; Jech, M.; Badisch, E.; Ditrói, F.; Kübler, A.; Mayrhofer, P.H. Evaluation of Wear Measurement with Radioactive Isotopes for DLC Coatings Affected by Abrasive Particles. *Tribol. Lett.* **2022**, *70*. [CrossRef]
6. NASA/JPL-Caltech/MSSS. Routine Inspection of Rover Wheel Wear and Tear. Available online: <https://mars.nasa.gov/resources/7809/routine-inspection-of-rover-wheel-wear-and-tear/> (accessed on 22 February 2022).
7. Rabinowicz, E. *Friction and Wear of Materials*; A Wiley-Interscience Publication, Wiley: Hoboken, NJ, USA, 1995.
8. Friedrich, K.; Reinicke, R.; Zhang, Z. Wear of polymer composites. *Proc. Inst. Mech. Eng. Part J. Eng. Tribol.* **2002**, *216*, 415–426. [CrossRef]

9. Watson, M.; Christoforou, P.; Herrera, P.; Preece, D.; Carrell, J.; Harmon, M.; Krier, P.; Lewis, S.; Maiti, R.; Skipper, W.; et al. An analysis of the quality of experimental design and reliability of results in tribology research. *Wear* **2019**, *426–427*, 1712–1718. [[CrossRef](#)]
10. Archard, J.F. Contact and Rubbing of Flat Surfaces. *J. Appl. Phys.* **1953**, *24*, 981–988. [[CrossRef](#)]
11. Schmitz, T.L.; Action, J.E.; Burris, D.L.; Ziegert, J.C.; Sawyer, W.G. Wear-Rate Uncertainty Analysis. *J. Tribol.* **2004**, *126*, 802–808. [[CrossRef](#)]
12. Burris, D.L.; Sawyer, W.G. Addressing Practical Challenges of Low Friction Coefficient Measurements. *Tribol. Lett.* **2009**, *35*, 17–23. [[CrossRef](#)]
13. Novak, R.; Polcar, T. Tribological analysis of thin films by pin-on-disc: Evaluation of friction and wear measurement uncertainty. *Tribol. Int.* **2014**, *74*, 154–163. [[CrossRef](#)]
14. Blau, P.J. How common is the steady-state? The implications of wear transitions for materials selection and design. *Wear* **2015**, *332–333*, 1120–1128. [[CrossRef](#)]
15. Kim, T.W.; Moon, S.M.; Cho, Y.J. Prediction of fretting wear using boundary element method. *Tribol. Int.* **2011**, *44*, 1571–1576. [[CrossRef](#)]
16. Rudnytskyj, A.; Krenn, S.; Vorlaufer, G.; Gachot, C. Influence of the 6061 Aluminium Alloy Thermo-Viscoplastic Behaviour on the Load-Area Relation of a Contact. *Materials* **2021**, *14*, 1352. [[CrossRef](#)]
17. Meng, H.; Ludema, K. Wear models and predictive equations: Their form and content. *Wear* **1995**, *181–183*, 443–457. [[CrossRef](#)]
18. Johansson, L. Numerical Simulation of Contact Pressure Evolution in Fretting. *J. Tribol.* **1994**, *116*, 247–254. [[CrossRef](#)]
19. Pödra, P.; Andersson, S. Simulating sliding wear with finite element method. *Tribol. Int.* **1999**, *32*, 71–81. [[CrossRef](#)]
20. McColl, I.; Ding, J.; Leen, S. Finite element simulation and experimental validation of fretting wear. *Wear* **2004**, *256*, 1114–1127. [[CrossRef](#)]
21. Söderberg, A.; Andersson, S. Simulation of wear and contact pressure distribution at the pad-to-rotor interface in a disc brake using general purpose finite element analysis software. *Wear* **2009**, *267*, 2243–2251. [[CrossRef](#)]
22. Hegadekatte, V.; Hilgert, J.; Kraft, O.; Huber, N. Multi time scale simulations for wear prediction in micro-gears. *Wear* **2010**, *268*, 316–324. [[CrossRef](#)]
23. Cavalieri, F.J.; Zenklusen, F.; Cardona, A. Determination of wear in internal combustion engine valves using the finite element method and experimental tests. *Mech. Mach. Theory* **2016**, *104*, 81–99. [[CrossRef](#)]
24. He, Z.; Hu, Y.; Zheng, X.; Yu, Y. A Calculation Method for Tooth Wear Depth Based on the Finite Element Method That Considers the Dynamic Mesh Force. *Machines* **2022**, *10*, 69. [[CrossRef](#)]
25. Mukras, S.M.S. Computer Simulation/Prediction of Wear in Mechanical Components. *Adv. Tribol.* **2020**, *2020*, 1–15. [[CrossRef](#)]
26. Molinari, J.; Ortiz, M.; Radovitzky, R.; Repetto, E. Finite-element modeling of dry sliding wear in metals. *Eng. Comput.* **2001**, *18*, 592–610. [[CrossRef](#)]
27. Hegadekatte, V.; Huber, N.; Kraft, O. Modeling and simulation of wear in a pin on disc tribometer. *Tribol. Lett.* **2006**, *24*, 51–60. [[CrossRef](#)]
28. Andersson, J.; Almqvist, A.; Larsson, R. Numerical simulation of a wear experiment. *Wear* **2011**, *271*, 2947–2952. [[CrossRef](#)]
29. Ilincic, S.; Vernes, A.; Vorlaufer, G.; Hunger, H.; Dörr, N.; Franek, F. Numerical estimation of wear in reciprocating tribological experiments. *Proc. Inst. Mech. Eng. Part J. Eng. Tribol.* **2013**, *227*, 510–519. [[CrossRef](#)]
30. Bortoleto, E.; Rovani, A.; Seriacopi, V.; Profito, F.; Zachariadis, D.; Machado, I.; Sinatora, A.; Souza, R. Experimental and numerical analysis of dry contact in the pin on disc test. *Wear* **2013**, *301*, 19–26. [[CrossRef](#)]
31. Kubiak, K.; Liskiewicz, T.; Mathia, T. Surface morphology in engineering applications: Influence of roughness on sliding and wear in dry fretting. *Tribol. Int.* **2011**, *44*, 1427–1432. [[CrossRef](#)]
32. Hutchings, I.; Shipway, P. *Tribology: Friction and Wear of Engineering Materials*; Butterworth-Heinemann: Oxford, UK, 2017.
33. Cameron-Plint TE77. Available online: [https://www.ltu.se/cms\\_fs/1.86403!/file/Poster\\_Cameron\\_Plint.pdf](https://www.ltu.se/cms_fs/1.86403!/file/Poster_Cameron_Plint.pdf) (accessed on 25 February 2022).
34. Rodiouchkina, M.; Lind, J.; Pelcastre, L.; Berglund, K.; Rudolphi, Å.K.; Hardell, J. Tribological behaviour and transfer layer development of self-lubricating polymer composite bearing materials under long duration dry sliding against stainless steel. *Wear* **2021**, *484–485*, 204027. [[CrossRef](#)]
35. ThorPlas Bearings Engineering Manual. Available online: [https://thordonbearings.com/docs/default-source/design/thorplas\\_engineering\\_manual.pdf?sfvrsn=f6c5c09a\\_42](https://thordonbearings.com/docs/default-source/design/thorplas_engineering_manual.pdf?sfvrsn=f6c5c09a_42) (accessed on 2 February 2022).
36. Rudnytskyj, A. Simulations of Contact Mechanics and Wear of Linearly Reciprocating Block-on-Flat Sliding Test. Master's Thesis, Department of Engineering Sciences and Mathematics, Luleå University of Technology, Luleå, Sweden, 2018.
37. Pennestri, E.; Rossi, V.; Salvini, P.; Valentini, P.P. Review and comparison of dry friction force models. *Nonlinear Dyn.* **2015**, *83*, 1785–1801. [[CrossRef](#)]
38. Mukras, S.; Kim, N.H.; Sawyer, W.G.; Jackson, D.B.; Bergquist, L.W. Numerical integration schemes and parallel computation for wear prediction using finite element method. *Wear* **2009**, *266*, 822–831. [[CrossRef](#)]
39. Cha, W.G.; Hammer, T.; Gutknecht, F.; Golle, R.; Tekkaya, A.E.; Volk, W. Adaptive wear model for shear-cutting simulation with open cutting line. *Wear* **2017**, *386–387*, 17–28. [[CrossRef](#)]
40. Pödra, P.; Andersson, S. Finite element analysis wear simulation of a conical spinning contact considering surface topography. *Wear* **1999**, *224*, 13–21. [[CrossRef](#)]

41. Ciavarella, M.; Hills, D.A.; Monno, G. The influence of rounded edges on indentation by a flat punch. *Proc. Inst. Mech. Eng. Part J. Mech. Eng. Sci.* **1998**, *212*, 319–327. [[CrossRef](#)]
42. Porter, M.; Hills, D. Note on the complete contact between a flat rigid punch and an elastic layer attached to a dissimilar substrate. *Int. J. Mech. Sci.* **2002**, *44*, 509–520. [[CrossRef](#)]
43. Waskom, M.L. seaborn: Statistical data visualization. *J. Open Source Softw.* **2021**, *6*, 3021. [[CrossRef](#)]
44. Hunter, J.D. Matplotlib: A 2D graphics environment. *Comput. Sci. Eng.* **2007**, *9*, 90–95. [[CrossRef](#)]
45. Plotly Technologies Inc. Collaborative Data Science 2015. Available online: <https://plot.ly> (accessed on 2 February 2022) .